JOURNAL OF CATALYSIS 96, 517–534 (1985)

Carbon Deposition and Methane Steam Reforming on Silica-Supported Ni–Cu Catalysts

C. A. BERNARDO,* I. ALSTRUP,† AND J. R. ROSTRUP-NIELSEN†

*Centro de Química Pura e Aplicada (INIC), Universidade do Minho, 4700 Braga, Portugal, and †Haldor Topsøe Research Laboratories, DK-2800 Lyngby, Denmark

Received December 3, 1984; revised June 12, 1985

Methane decomposition and steam reforming were studied over silica-supported copper–nickel alloy catalysts. Hydrogen chemisorption and X-ray photoelectron spectroscopy (XPS) measurements showed copper surface segregation after reduction at 773 K. The carbon formation/gasification equilibrium was the same for the alloy catalysts as for monometallic nickel catalysts except at the highest copper concentration (80 at.% Cu). The rate of carbon formation, for more than 10 at.% Cu, was more strongly decreased by alloying with Cu than the rate of steam reforming, which followed approximately the decrease in hydrogen capacity. On samples with less than 80 at.% Cu the carbon was deposited mainly as filaments with a metal particle at the end and with approximately the same diameter as the metal particle. At 80 at.% Cu thinner filaments of a new type were observed. A kinetic expression describing the rate of methane decomposition at low hydrogen pressure over the catalysts with 10 at.% Cu or lower indicates that a surface reaction step is rate controlling.

INTRODUCTION

The production of pure hydrogen and synthesis gas by steam conversion of methane, the main component of natural gas, is an important and well-known industrial process. Supported nickel catalysts are commonly used in this reaction and their activity and deactivation patterns have been widely studied. The operation with minimum oxygen-to-carbon ratios can lead to the formation of carbon either by decomposition of methane or carbon monoxide. Carbon deposition may decrease the activity of the catalysts and can cause severe operational problems in the reformer. Various methods have been used to prevent carbon deposition, namely, the use of additives and the control of the size of the metallic particles of the catalyst and of the operational conditions (*1*).

Recently, it was found that the coverage of the nickel surface by sulfur, above 70% of full coverage, inhibits the rate of carbon formation more than the rate of steam reforming. This effect was explained assuming that the nucleation of carbon involves a larger number of active nickel surface sites than the steam reforming reaction (*2*).

One method of controlling the extension of the active surface domains is the alloying of nickel with a metal inactive for the decomposition of methane. Copper appears to be such a metal, as it does not chemisorb methane (*3*), shows no activity for carbon deposition from aliphatic hydrocarbons at temperatures below 1073 K (*4*), and, in alloys with nickel, decreases the tendency for deactivation (5). In addition to this, Barcicki *et al.* (*6*) state that the addition of 0.02% (w/w) of copper to alumina-supported nickel catalysts increases significantly the rate of methane steam reforming.

The study of supported Ni–Cu systems is of great interest per se. In spite of the many studies published about catalytic Ni–Cu alloys, some controversial points remain (*7*). Although it is established that, at equilibrium, the surface of *massive* alloys and films is enriched with copper as compared with the bulk, the situation of *supported* alloys is less clear. It is conceivable that

0021-9517/85 $3.00

small alloy particles may not have the same surface-to-bulk composition relation as massive samples. Surface segregation could be enhanced due to lower surface atom coordination, while, on the other hand, the limited supply from the bulk of small particles could result in limited segregation or, in the case of phase separation, in island formation on the surface.

Dalmon (*8*) and Vass and Contescu (*9*) concluded, on the basis of hydrogen chemisorption and magnetic measurements, that the surface composition of Ni–Cu alloys supported on silica and kieselguhr, respectively, was the same as that of the bulk. On the other hand, Maskos and van Hooff (*10*) and Cale and Richardson (*11*) stated that the surfaces of Ni–Cu alloys supported on zeolites and silica, respectively, were enriched in Cu. Vass and Contescu (*9*) attributed these differences to the methods of catalyst preparation and to the nature of the support.

Recently, Bajpai *et al.* (*5*) observed that the capacity for hydrogen chemisorption of alumina-supported Ni–Cu catalysts decreased more than linearly with increasing Cu content. To reconcile this observation with the nonenrichment conclusion of Dalmon (*8*), they suggested that large nickel ensembles are necessary for the chemisorption of hydrogen and that the number of such ensembles drops rapidly with increasing copper concentration.

The catalytic effect of Ni–Cu alloys in a number of reactions was reviewed by Khulbe and Mann (*7*) and by Ponec (*12*). According to Ponec (*12*), all the reactions can be divided into two groups: *Type I*, comprising reactions for which the specific catalytic activities of alloys with medium-range Cu concentrations are about the same as for pure nickel, and *Type II*, comprising reactions for which the specific catalytic activities of the alloys are more than one order of magnitude lower than those of pure nickel. Briefly, the first type corresponds to reactions where C–H or O–H bonds are broken or formed, while the second type corresponds to reactions where C–C or C–O bonds are broken.

Very few studies of reactions on supported Ni–Cu alloys have been reported. Contrary to Barcicki *et al.* (*6*), Bajpai *et al.* (*5*) observed a much lower methanation activity for alumina-supported Ni–Cu catalysts than for the same catalysts without copper. For ethene hydrogenation, Vass and Contescu (*9*) also observed a decrease in the activity, when adding up to 20% copper to nickel supported on kieselguhr.

Luyten *et al.* (*13*) studied the methanation reaction over silica-supported Ni–Cu catalysts. Dalmon and Martin (*14, 15*) studied methanation, hydrogenolysis of alkanes, C_6H_6 hydrogenation, and CH_4/D_2 exchange over silica-supported Ni–Cu catalysts and correlated the changes in the activity with changes in the probability of ensembles of Ni surface atoms.

In the present work we report the study of the properties of a range of silica-supported Ni–Cu catalysts and of their activity for carbon deposition and steam reforming.

EXPERIMENTAL

1. *Catalyst Preparation*

$Ni–Cu/SiO_2$ catalysts were prepared by "dry" impregnation. The required amounts of nickel and copper nitrates were dissolved in a volume of water equal to the measured pore volume of the support material (Cab-O-Sil H5). The solution and the support material were mixed together by vigorous stirring in a mortar until the mixture became a thick, homogeneous liquid. It was then dried at room temperature and finally calcined at 773 K for 3 h. The catalysts were reduced at 773 K in H_2 for 44 h.

Catalysts were prepared with 20 wt% total nickel plus copper and nominal bulk copper concentrations in the metallic phase of 0, 0.1, 1, 10, 25, 50, 80, and 100 at.%.

2. *Characterization*

The reduced samples were characterized by hydrogen chemisorption, hydrogen sul-

fide chemisorption (sulfur capacity measurement), X-ray diffraction, electron microscopy, and X-ray photoelectron spectroscopy.

Hydrogen chemisorption. Hydrogen chemisorption measurements were carried out in a volumetric system with a Texas Instruments precision pressure gauge. The samples were rereduced at 773 K for 16 h in the chemisorption system, followed by a 1-h evacuation at 773 K to a final pressure of about 3×10^{-4} Pa. The total H_2 uptake was measured at 298 ± 3 K and 0.2–30 kPa. The samples were then evacuated to about 4×10^{-4} Pa for 1 h at this temperature and a new isotherm was measured. The difference between the two isotherms is denoted as "strongly chemisorbed" hydrogen (*16, 17*).

Sulfur capacity. Samples of the catalysts were saturated with sulfur by exposure to a flow of hydrogen containing 10–20 ppm H_2S for 96 h at 825 K. The sulfur capacity (*1*) was then determined by analyzing the amount of sulfur chemisorbed using Gustafsson's method (*18*).

X-Ray powder diffraction (XRPD). X-Ray diffraction measurements were carried out using Cu$K\alpha$ radiation. The lattice constants of the metal particles of the catalyst samples were measured from the angle of the (111), (200), and (220) reflections. The diffraction angle was calibrated from measurements on natural quartz. The mean crystallite size of the metal particles was calculated from the width of the (111), (200), and (220) diffraction peaks, corrected for $K_{\alpha 1 \alpha 2}$ and instrumental broadening by using the methods described by Klug and Alexander (*19*).

Electron microscopy (EM). The morphology of the carbon formed on the catalyst samples was studied by means of a JEOL 100-CX electron microscope. The composition of the metal particles of some of the catalyst samples was analyzed by means of the KEVEX energy dispersive X-ray spectrometer of the microscope after carbon deposition. These measurements were made in the STEM-SCAN mode with an analyzed area in the range 5–10 nm.

X-Ray photoelectron spectroscopy (XPS). XPS spectra were taken for several of the freshly reduced samples by means of a modified V.G. Scientific ESCA 3 spectrometer. After reduction, the samples were brought into the spectrometer without contact with air through a stainless-steel high-vacuum glovebox connected to the preparation chamber of the apparatus. Al$K\alpha$ radiation was used for the excitation of the surface atoms. A constant-pass energy of 50 eV and 4-mm slitwidth was used for all recordings.

The intensities of the Ni 2*p*, Cu 2*p*, Si 2*p*, and O 1*s* peaks were determined by measuring the areas bounded by the spectral curve and a linear background tangent to the curve, at a point on each side of the two spin–orbit component peaks of the 2*p* spectra or on each side of the O 1*s* peak.

3. Reactor System and Reactants

The reactor system consisted of a microbalance (C.I. Electronics, MK2B) and associated flow reactor, heated lines, furnaces, and temperature controllers (*2, 4*). The composition of the outlet gas was determined by gas chromatography, thus allowing simultaneous measurements of the rates of the reforming and carbon deposition reactions. The latter rates were determined from the slope of the curves drawn by the microbalance recorder.

A constant steam flow was obtained by direct hydrogen reduction of copper oxide in an on-line heated reactor. The other gases were available in bottles. Methane contained less than 0.05% impurities (mainly CO_2), with no higher hydrocarbons detectable by gas chromatographic analysis.

A single catalyst pellet (4 × 4 mm cylinder, approx. 60 mg) was placed in a quartz basket suspended from the microbalance.

All the experiments were performed at atmospheric pressure and with total flows varying from 0.61 to 0.90 mol h^{-1}.

Except where otherwise stated in the captions of the figures most of the experiments were performed with the same partial pressure of reactants (P_{CH_4} ca. 13 kPa, P_{H_2} ca. 7 kPa, P_{H_2O} ca. 3 kPa). Nitrogen was used as diluent throughout this work.

Prior to the reaction pure hydrogen was flushed through the reactor at the working temperature, until there was complete reduction of the catalyst.

RESULTS

1. *Characterization of Catalysts*

1.2. X-Ray powder diffraction (XRPD). The X-ray diffraction spectra of the reduced catalysts showed only one metal phase to be present, when the copper content was less than that of nickel. The alloy had a composition which was equal to the nominal composition within the accuracy of the determination from the lattice parameter.

The spectra of the catalysts with 50 and 80 at.% Cu showed the existence of two metal alloy phases.

The peaks observed for the catalyst with 50 at.% Cu showed that ca. 92% of the metal was present as an alloy with about 47 at.% Cu and the rest as an alloy with about 95 at.% Cu. For the catalyst with 80 at.% Cu, the spectra showed that ca. 40% of the metal was present as an alloy with ca. 59 at.% Cu and the rest as pure Cu.

TABLE 1

Mean Particle Diameters from XRPD, Sulfur Capacities, and Total Metal Surface Areas

Cu at.%[a]	$\bar{D}_{XRPD}$ (nm)	S (μg/g cat)	A_s (m^2/g cat)	A_{XRPD} (m^2/g cat)	A_{XPS} (m^2/g cat)
0	19.1	2050	4.6[b]	4.6	4.6
0.1	19.0	1940	4.4	4.6	—
1	17.5	1880	4.5	5.0	—
10	15.0	2010	5.0	5.8	4.3
25	16.3	1860	4.8	5.4	5.4
50	20.4	1680	4.3	4.3	4.2
80	18 (40%) 45 (60%)	1390	3.6	3.1	3.8
100	32	1760	4.6[b]	2.7	4.6

[a] $\frac{Cu}{Cu + Ni} \cdot 100$.

[b] From the formula $\bar{D} = V/A$ the mean particle diameter is calculated to be ca. 30 nm for the two monometallic catalysts, i.e., approximately equal to $\bar{D}_{XRPD}$ for the Cu/SiO_2 catalyst but ca. 1.5 times $\bar{D}_{XRPD}$ for the Ni/SiO_2 catalyst.

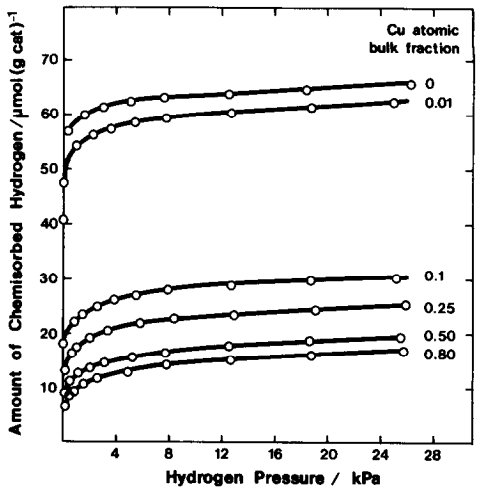

FIG. 1. Hydrogen isotherms. Total uptake at 298 ± 3 K for x = 0, 0.01, 0.1, 0.25, 0.5, 0.8, where x = Cu atomic bulk fraction of the metal particles.

The mean particle diameters $\bar{D}_{XRPD}$, determined from the widths of the diffraction peaks, are shown in Table 1. For the catalyst with 80 at.% Cu two values, corresponding to the two metal phases, are shown.

1.2. Hydrogen chemisorption. Some of the hydrogen isotherms measured at room temperature are shown in Fig. 1. The uptake (μmol/g cat) of total and weakly adsorbed hydrogen, respectively, were determined as a function of hydrogen pressure. The amount of strongly chemisorbed hydrogen was determined by taking the differences between these two curves. It is almost independent of pressure. The values obtained for the strong chemisorption at P_{H_2} = 133 Pa are plotted in Fig. 2 as a function of the nominal bulk Cu concentration of the metal particles.

The hydrogen chemisorption results presented in this study agree quite well with those reported previously for unsupported (*16, 17, 20*) and alumina-supported (*5*) Ni–Cu alloys, but they differ from those obtained by Dalmon (*8*) for Ni–Cu/SiO_2 alloy catalysts.

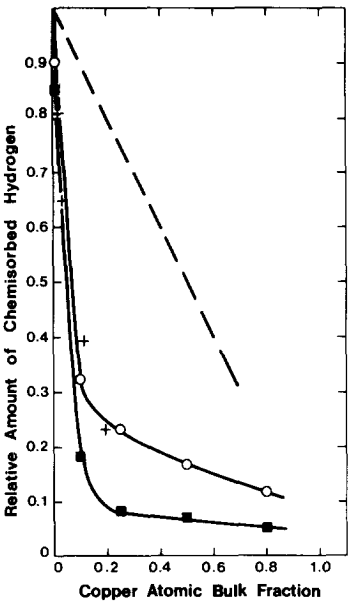

FIG. 2. Relative hydrogen uptake at 298 ± 3 K. (○) Total uptake; (■) strong uptake; (+) Bajpai *et al.* (*5*); (---) Dalmon (*8*).

The hydrogen capacity of alloys cannot be converted unambiguously into a nickel surface area. Hence, in the present work, the normalized rates are just referred to the capacity of "strongly chemisorbed" hydrogen.

1.3. Sulfur capacity. The sulfur capacities (μg S/g catalyst), corrected for sulfur uptake by the support (20 μg S/g support), are shown in Table 1.

From the sulfur capacities the metal particle areas A_s (m^2 per g catalyst) shown in Table 1 were calculated by assuming the same copper segregation as in massive alloy samples. In the calculations, the saturation values for sulfur chemisorption were taken to be 449 μg S/(m^2 Ni) and 384 μg S/(m^2 Cu), which correspond to the mean values for the (111), (100), and (110) surfaces. (*21*). On the basis of the sulfur capacity, the mean particle diameter for the Ni/SiO_2 catalyst was estimated to be ca. 30 nm. This value is larger than that found by XRPD (see Table 1). A similar discrepancy between XRPD and chemisorption data has been reported before (*1*, *22*).

1.4. X-Ray photoelectron spectroscopy (XPS). The electron binding energies (BE) of the Ni $2p_{3/2}$, Cu $2p_{3/2}$, and O 1*s* peaks, were corrected for charging by subtracting a constant energy amount so that BE(Si 2*p*) becomes 103.6 eV. The BE's for Ni and Cu were equal to the values for the pure metals within the accuracy of the measurements (±0.3 eV). The intensity ratios $I_{Ni\,2p}/I_{Si\,2p}$, $I_{Cu\,2p}/I_{Si\,2p}$, and $I_{O\,1s}/I_{Si\,2p}$ are shown in Table 2.

The metal areas A_{XPS} (m^2/g cat) were calculated from the intensity ratios by using the metallic areas of the monometallic catalysts determined from the sulfur capacities as described above. The calculations of the A_{XPS} of the alloy catalysts were based on the simplest possible model, assuming a homogeneous surface layer of thickness *d* and a homogeneous bulk phase.

The following expression for the Cu–Ni intensity ratio can then be derived:

$$\frac{I_{Cu}}{I_{Ni}} = \frac{S_{Cu}}{S_{Ni}} \cdot \frac{\phi}{1-\phi} \qquad (1)$$

with

$$\phi = x_s + (x_b - x_s)\exp(-d/\lambda \sin\theta), \qquad (2)$$

where x_s and x_b are the Cu atomic ratios in the surface layer and in the bulk, respectively, λ is the inelastic mean free path of the electrons (the difference between Ni 2*p*

TABLE 2

XPS Intensity Ratios from Ni 2*p*, Cu 2*p*, Si 2*p*, and O 1*s* Intensities

Cu at.%[a]	I_{Ni}/I_{Si}	I_{Cu}/I_{Si}	I_O/I_{Si}	I_{Cu}/I_{Ni}	$\frac{2x_b}{1-x_b}$ [b]
0	0.115	0	6.9	0	0
10	0.079	0.061	6.9	0.77	0.22
25	0.086	0.099	6.5	1.16	0.67
50	0.053	0.102	7.0	1.91	2.0
80	0.029	0.133	6.9	4.6	8.0
100	0	0.231	6.7	∞	∞

[a] $\frac{Cu}{Cu + Ni} \cdot 100$.

[b] Theoretical Cu–Ni intensity ratio for homogeneous metal particles (see text).

and Cu 2*p* electrons is neglected), and θ is the escape angle of the emitted electrons. S_{Cu} and S_{Ni} are the sensitivity factors for Cu 2*p* and Ni 2*p* electrons, respectively. Then, for a homogeneous Ni–Cu alloy:

$$\left(\frac{I_{Cu}}{I_{Ni}}\right)_{hom} = \frac{S_{Cu}}{S_{Ni}} \cdot \frac{x_b}{1 - x_b}. \quad (3)$$

By assuming the intensities of the Cu and Ni lines to be proportional to the relative concentrations multiplied by the metal area per gram catalyst, the following expressions are obtained:

$$A_{XPS} = A_s(x_b = 1) \cdot (I_{Cu}/I_{Cu,1}) \cdot [1 + (S_{Cu}/S_{Ni})(I_{Ni}/I_{Cu})] \quad (4)$$

or

$$A_{XPS} = A_s(x_b = 0) \cdot (I_{Ni}/I_{Ni,0}) \cdot [1 + (S_{Ni}/S_{Cu})(I_{Cu}/I_{Ni})]. \quad (5)$$

Similarly, for homogeneous alloys (without surface layer):

$$A_{XPS} = A_s(x_b = 1) \cdot (I_{Cu}/I_{Cu,1}) \cdot \frac{1}{x_b} \quad (6)$$

and

$$A_{XPS} = A_s(x_b = 0) \cdot (I_{Ni}/I_{Ni,0}) \cdot \frac{1}{1 - x_b}, \quad (7)$$

where $I_{Cu,1}$ and $I_{Ni,0}$ are the intensities for monometallic copper and nickel catalysts, respectively.

The sensitivity factor ratio S_{Cu}/S_{Ni} in the expressions (1), (4), and (5) can be determined from Table 2, using the two intensity ratios $(I_{Cu}/I_{Si})_{x_b=1}$ and $(I_{Ni}/I_{Si})_{x_b=0}$ for the monometallic catalysts and the areas determined by the sulfur capacity measurements:

$$\frac{S_{Cu}}{S_{Ni}} = \frac{I_{Cu}}{I_{Si}} \cdot \frac{I_{Si}}{I_{Ni}} \cdot \frac{A_{Ni}}{A_{Cu}} \simeq 2.0. \quad (8)$$

Using this value and the formulas (4) or (5), the A_{XPS} values shown in Table 1 are obtained. If no surface enrichment layers are present, the intensity ratio I_{Cu}/I_{Ni} would be $(2.0) \cdot x_b/(1 - x_b)$. This factor is shown in Table 2.

2. *Carbon Deposition*

2.1. Equilibrium tests. A series of experiments was performed to assess the characteristics of the carbon formed on these alloy catalysts via the reaction

$$CH_4 \rightleftarrows C + 2H_2 \quad (9)$$

using mixtures of methane and hydrogen.

The equilibrium quotient

$$K_e = \frac{(P_{H_2})^2}{P_{CH_4}} \quad (10)$$

was calculated using the partial pressures corresponding to the onset of carbon formation, i.e., the methane pressure above which carbon is formed for a fixed hydrogen pressure and below which carbon is removed. The K_e values were determined at reversible conditions and, accordingly, they can be considered as equilibrium constants.

Figure 3 shows the value of K_e as a function of the temperature for the entire range of copper contents studied. A straight line was fitted by linear regression analysis to the whole data distribution with a relative error smaller than 5%. The quotient ratios for the reaction on the 80 at.% Cu catalyst were consistently smaller than those for the other catalysts. On the other hand, there was no systematic difference between the data corresponding to the 100% Ni and to the Ni–Cu alloy catalysts. The temperature dependence of K_p, the constant corresponding to the equilibrium of methane and hydrogen with graphite, is also presented in Fig. 3.

Values for the free energy deviation from graphite data:

$$\Delta G_c = RT \ln(K_p/K_e) \quad (11)$$

which can be obtained from the two lines in Fig. 3, can be correlated with the reciprocals of the maximum diameters of the nickel particles on top of carbon whiskers. These deviations were attributed to the contribution of the surface energy of the whiskers (*1*).

At 773 K, for instance, the present data

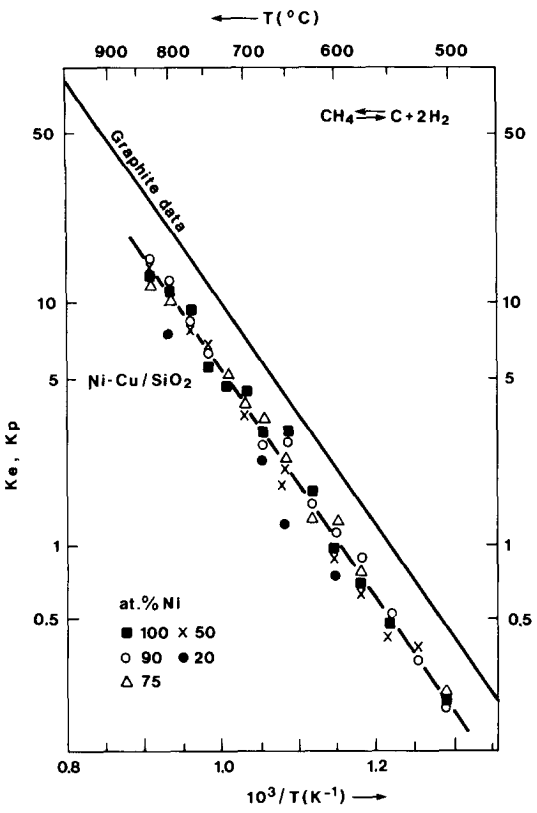

FIG. 3. Equilibrium for methane decomposition on Ni–Cu/SiO_2 alloy catalysts. K_p from graphite data, K_e as in Eq. (10) (pressures in atm). Total flow ca. 0.8 mol h^{-1}. Points obtained by interpolation between carbon deposition and gasification rates.

give ΔG_c = 4.45 kJ mol^{-1}. Then, from Ref. (*1*), this corresponds to an equivalent diameter of ca. 50 nm obtained for the largest particles present in the carbon deposits. This is in agreement with the diameter of the largest nickel crystals observed in the electron microscope (Table 3). The bigger values of ΔG_c determined for the 80 at.% Cu catalysts may be explained either by smaller metallic particles or by a less-ordered structure of the carbon formed (see below).

2.2. Morphology of carbon deposits. X-Ray microanalysis in the electron microscope showed that the copper concentrations of the metallic particles do not change significantly with the carbon deposition. In most of the samples with carbon deposits the typical carbon whisker structure with a less dense core and a metallic particle at the top (*1, 4, 23*) was observed in the electron microscope (Table 3).

The deposits formed on the 80 at.% Cu catalyst showed, however, a different structure with various filaments of amorphous carbon attached to the same metallic particle. Similar "octopus" carbon has also been observed by Rostrup-Nielsen in deposits formed on nickel catalysts with high sulfur coverages (*2, 24*). Figure 4 shows micrographs of typical "whisker" and "octopus" carbon structures.

TABLE 3

Electron Microscopy and X-Ray Diffraction Analysis of Fresh and Deposited Catalysts

Cu at.%[a]	$\bar{D}_{XRPD}$ (nm)		$\bar{D}_{EM}$ (nm)		EM observ. deposited catalyst
	Fresh catalyst	Deposited catalyst[b]	Fresh catalyst	Deposited catalyst	
0	19.1–21.5	40.7	15.0–50.0	—	Whisker carbon
10	15.0–16.7	26.8–50.6	—	—	Whisker carbon
25	16.3	19.8	~25.0	70.0–140.0	Whisker carbon
50	20.4	—	~60.0	~60.0	Whisker carbon
80	18–45	—	—	—	"Octopus" carbon (amorphous structure)

[a] $\frac{Cu}{Cu + Ni} \cdot 100$.

[b] Corresponding to the (220) peak.

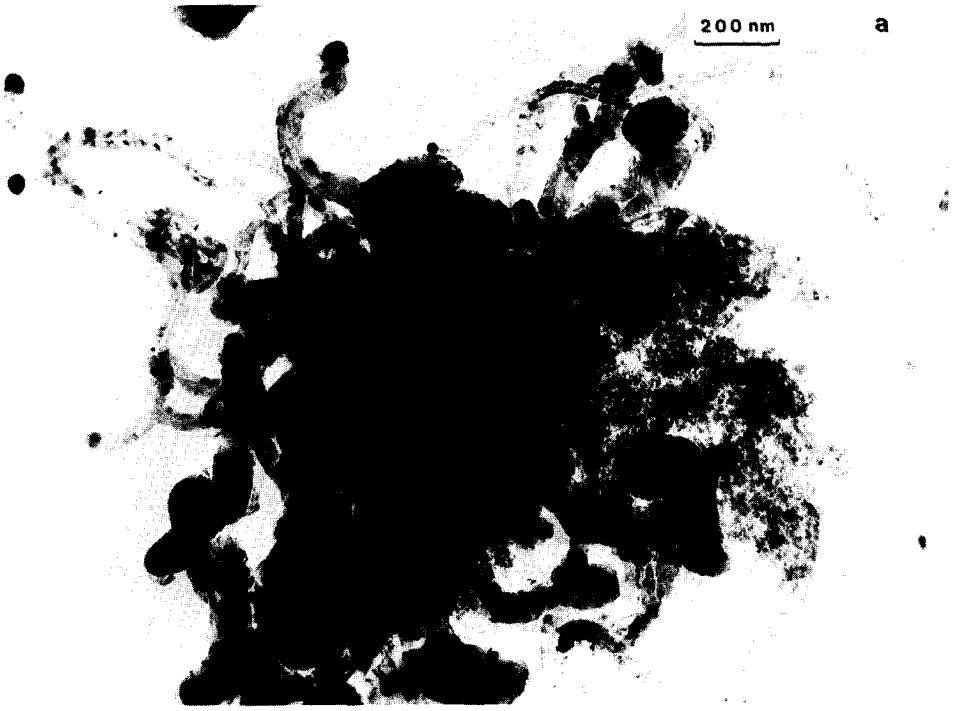

FIG. 4. Electron micrographs of the carbon deposits formed: (a) on the 10 at.% Cu catalyst (whisker carbon); (b) on the 80 at.% Cu catalyst ("octopus" carbon); (c) on the 100 at.% Cu catalyst ("pneumatic tube" carbon).

"Octopus" carbon was observed in all the deposits formed on the 80 at.% Cu catalysts, and this may well explain the higher deviations in the free energy referred to above. In fact, in contrast to the whisker carbon structure, the "octopus" structure is characterized by carbon filaments with diameters smaller than those of the nickel particles to which they are attached. Therefore, a higher contribution from surface energy is to be expected in this case.

On the 100% Cu/SiO_2 catalyst long and thin, almost transparent carbon filament tubes with elongated copper particles inside were observed after carbon deposition (see Fig. 4c).

2.3. Carbon deposition rates. The rates of carbon deposition, measured for various values of temperature and partial pressure of methane and hydrogen, are presented in Fig. 5a. Figure 5b shows the same rates normalized by the hydrogen chemisorption capacity. As for previous experiments with nonalloyed nickel catalysts (*25*), the rates were constant with time after a short, temperature-dependent, induction period. After the establishment of the steady state, changes in reactant pressures or temperature lead very rapidly to a new constant value of the rate.

Figure 5 summarizes the data for the temperature dependence of the rate for the whole range of copper concentrations studied. The relative activities of the various catalysts are maintained when the rates are normalized by referring to the capacity for strongly chemisorbed hydrogen. For the 100% copper sample, carbon is only formed above 998 K, supposedly by a noncatalytic reaction (*4*). Figure 5 indicates that the process of carbon formation at the higher copper concentrations is strongly sensitive to the surface concentration of active nickel sites (see also Fig. 8).

Carbon deposition experiments were performed at constant temperature and fixed

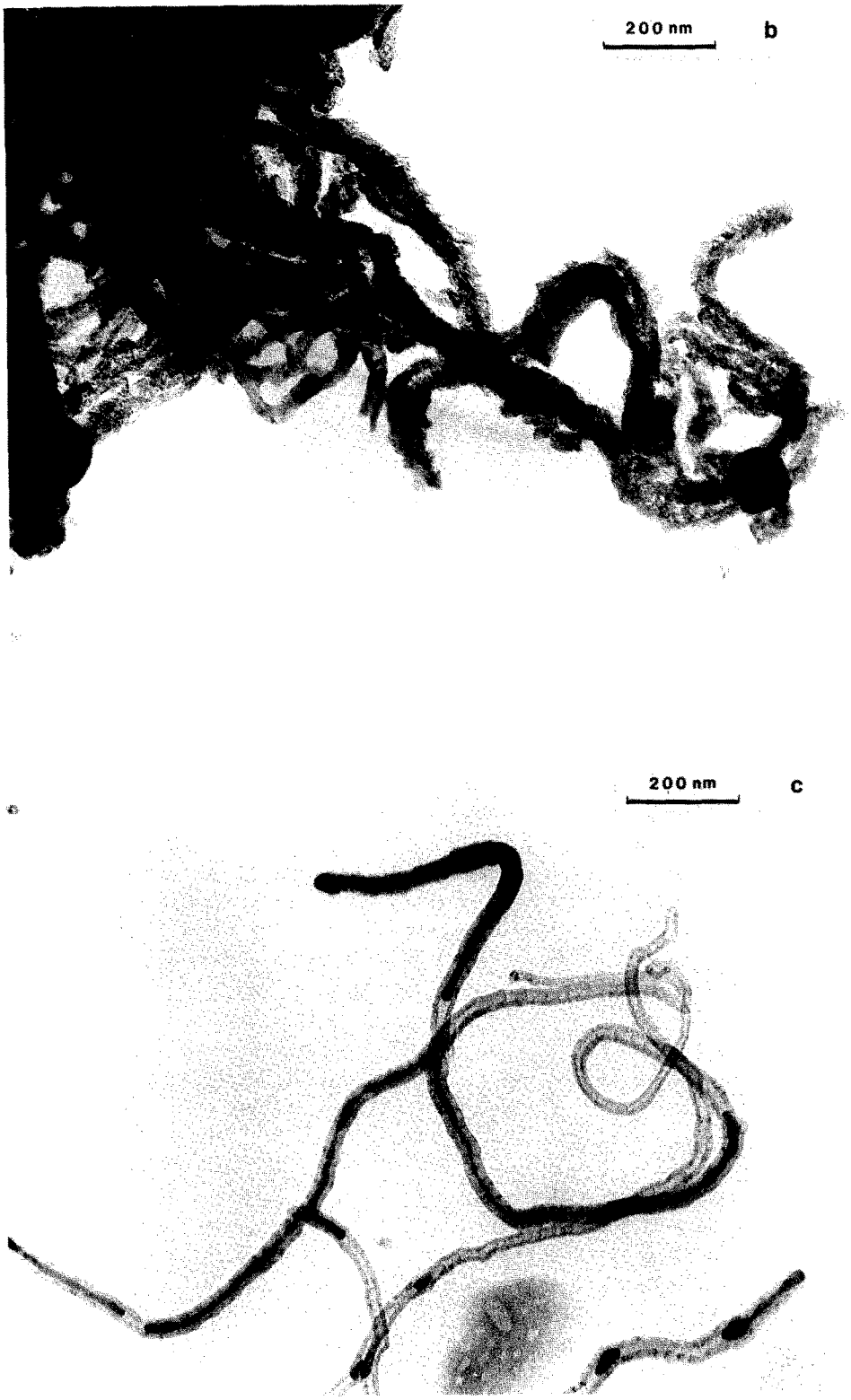

FIG. 4—*Continued.*

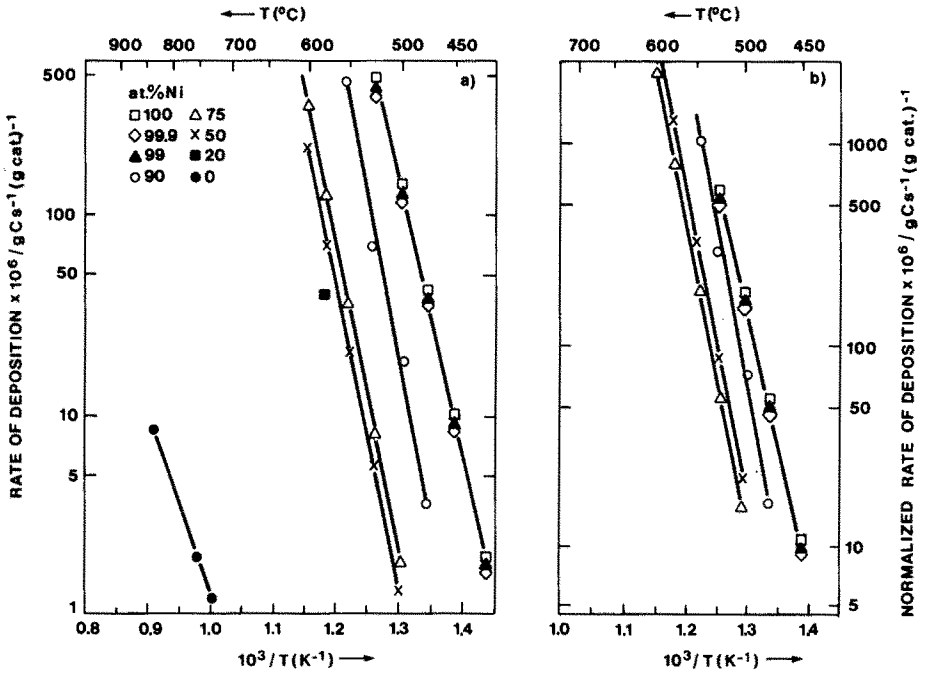

FIG. 5. Dependence on temperature of the rates of carbon formation from methane. Rates normalized: (a) by the catalyst weight; (b) by the relative amount of strongly chemisorbed hydrogen. Conditions: P_{CH_4} = 13.2 kPa; P_{H_2} = 7.1 kPa; N_2 as balance. Total flow ca. 0.7 mol h^{-1}.

pressure of one of the reactants. Results for the 1 and 10 at.% Cu catalysts are presented in Figs. 6a and b, respectively. Data were also obtained in the same type of experiments for 50 at.% Cu catalyst.

3.6. Steam reforming and carbon deposition. Simultaneous steam reforming and carbon deposition rates were determined in the reactor microbalance system for Ni–Cu catalysts with 0, 1, 10, and 50 at.% Cu and reactor temperatures from 748 to 998 K. Mass balances with respect to carbon agreed quite well for all the experiments, typically within ±1.5%.

Gas chromatographic analysis of the outlet gases, when steam was present, showed that the Cu content had a strong influence on the conversion of methane but practically no effect on the CO/CO_2 ratio.

The rates, normalized by the hydrogen chemisorption capacity, are presented in Fig. 7, plotted against the catalyst temperature. The experiments were affected by heat transfer restrictions in the gas film surrounding the catalyst particle. Hence, the catalyst temperature had to be estimated using a correlation for the apparatus, established in earlier studies (*2*), which involves the gas and reactor wall temperatures.

The influence of pore diffusion on the reforming rates is reflected by the data in Fig. 7, at temperatures above 798 K, for the 100% Ni catalyst (note that, although not shown in the figure, the nonnormalized rates for the alloyed catalysts were well below those for the 100% Ni catalyst). This influence is confirmed when calculating the effectiveness factor, η (at 998 K, for instance, for an assumed D_{eff} = 0.1 m^2 h^{-1}, η = 0.7).

It can be observed in Fig. 7 that the reforming rates are consistently and significantly higher than the rates for carbon deposition. The carbon deposition curves show a maximum above which the rates decrease sharply with temperature. A similar

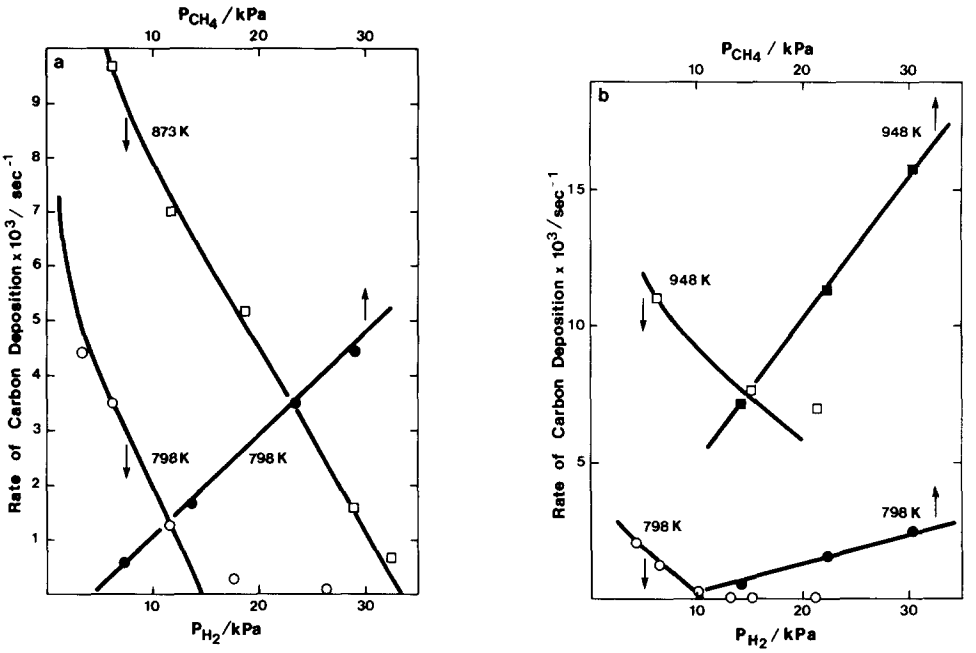

FIG. 6. Rates of carbon formation on Ni–Cu/SiO_2 alloy catalysts by decomposition of methane at constant methane pressure and at constant hydrogen pressure: (a) 1 at.% Cu catalyst; (b) 10 at.% Cu catalyst. Points are experimental values. Curves are calculated using Eq. (13) and the parameter values in Table 4. Conditions: (a): (○) P_{CH_4} = 22 kPa; (●) P_{H_2} = 6.5 kPa; (□) P_{CH_4} = 18 kPa. (b): (○) P_{CH_4} = 22 kPa; (●) P_{H_2} = 6 kPa; (□) P_{CH_4} = 22 kPa; (■) P_{H_2} = 6 kPa. Total flow in both cases ca. 0.8 mol h^{-1}.

rate maximum with temperature is not observed for the reforming reaction.

The activities of the different Ni–Cu catalysts for the deposition of carbon in the presence of steam (Fig. 7) are not very different when the rates are referred to the hydrogen capacity, showing that the dependence on copper content is smaller than for CH_4 decomposition without steam.

The behavior of the catalysts in the reforming reaction is quite different as the rates, normalized in the same way, show a complex dependence on the concentration of copper. This difference can be better understood if the data are presented in the form shown in Fig. 8, in which the ratio of the rates for alloy and 100% Ni catalysts is plotted as a function of the copper content of the alloy catalysts. It is clearly seen that, for fixed temperature and reactant concentrations, the reforming rates decrease much less than the carbon deposition rates when the copper content increases.

DISCUSSION

1. Structure of Ni–Cu Alloy Catalysts

Previous studies of supported Ni–Cu catalysts have shown that proper characterization of alloy catalysts is considerably more difficult than for monometallic catalysts. Some of the standard methods of catalyst preparation have been shown to result in incomplete alloying (*26*) or in the formation of more than one alloy phase (*27*). A major problem with alloy catalysts is that a separate analysis of the composition of the surface of the metal particles is required due to the probable surface segregation of one of the components. In the present work hydrogen chemisorption and XPS were used to settle this question.

The analysis of the X-ray diffraction spectra with respect to the number of metal phases and their compositions are in agreement with the results reported by Soma-Noto and Sachtler (*27*) for a range of

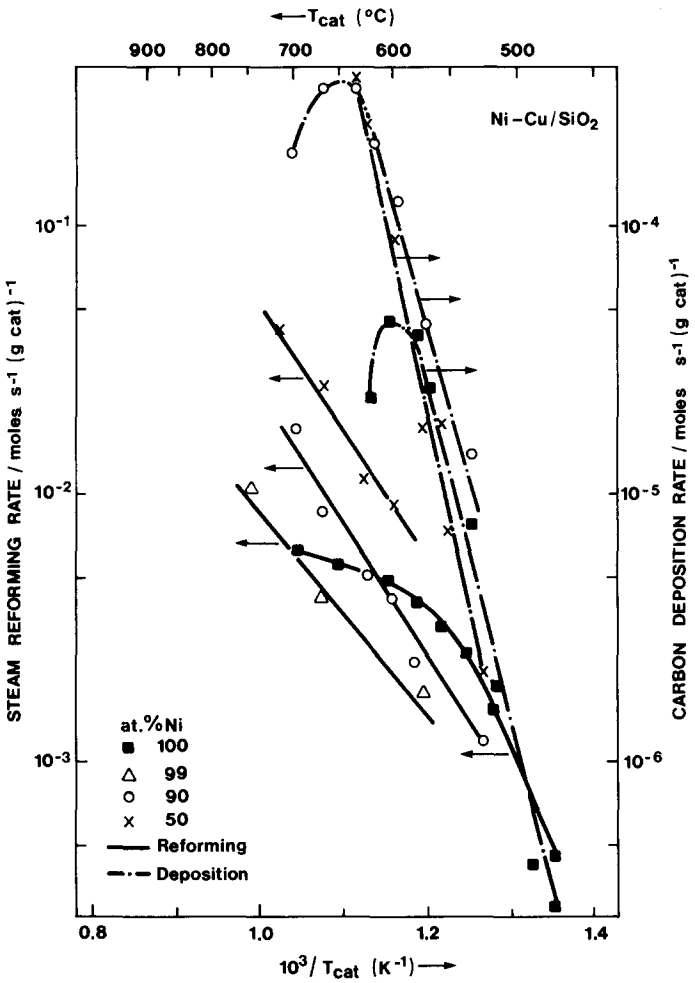

FIG. 7. Dependence on temperature of the rates of simultaneous carbon formation (right-hand side ordinates) and steam reforming (left-hand side ordinates). Rates normalized by the relative amount of strongly chemisorbed hydrogen. Conditions: P_{CH_4} = 13.2 kPa; P_{H_2} = 6.8 kPa; P_{H_2O} = 3.0 kPa; N_2 as balance. T_{cat} estimated from $aT_{cat}^4 + bT_{cat} = aT_w^4 + bT_{gas} - Q$. T_w is the wall temperature of the reactor (T in Kelvin), Q (kJ/mol) is heat absorbed by the reaction, $a = 1.36 \times 10^{-4}$ and $b = 5.04 \times 10^{-2}$ (from Ref. (2)).

Ni–Cu/SiO_2 catalysts prepared by impregnation. They found that catalysts with more than 50% Cu consist of two phases, a Cu-rich alloy (ca. 95% Cu) and a Ni-rich alloy (ca. 65% Ni). The proportion of the two phases varied with total Cu content. The particle sizes (12–15 nm) calculated by those authors from the width of the peaks are in good agreement with the present results, considering that a higher reduction temperature was used in this work. X-Ray diffraction, chemical analysis, and XPS show, in agreement with the results obtained by Robertson *et al.* (*26*), that the reduction conditions used in the present work result in completely reduced Ni–Cu/SiO_2 catalysts.

The understanding of hydrogen chemisorption on Ni–Cu alloys at the relatively high pressures (0.1–10 kPa) applied in the volumetric chemisorption measurements is far from complete. However, from the surface analysis by electron spectroscopy (AES and XPS) and ion scattering (ISS) of

massive Ni–Cu alloys, it has been shown (*12*) that the strong drop in hydrogen chemisorption capacity with copper content is due to surface enrichment in copper.

In the present study, the very good agreement of the hydrogen chemisorption results with those reported for unsupported Ni–Cu alloys (*16, 17, 20*), can be taken as evidence of surface enrichment in copper of the metal particles of the reduced Ni–Cu/SiO_2 catalysts. This conclusion is supported by the XPS results. The intensity ratios for the Cu 2*p* and the Ni 2*p* peaks are significantly larger for the 10 and 25 at.% Cu samples than would be expected for homogeneous particles.

At the higher Cu concentrations, the presence of more than one metallic phase complicates the interpretation. It is reasonable, however, that the intensity ratio observed for the 80 at.% Cu sample is smaller than that expected for a homogeneous sample, as a considerable part of the copper is present in particles with diameters larger than the escape depth of the photoelectrons.

In the analysis of the hydrogen chemisorption results it was assumed that the metal area per gram of catalyst was the same for all the samples. This assumption is justified by the X-ray diffraction peak broadening and the XPS intensity measurements which are in reasonable agreement except for the 100% Cu and 10 at.% Cu samples. In the latter case, an anomalously broad (200) diffraction peak corresponds to a fairly large metal area, while the XPS intensities correspond to an area below average. The metal area of the 100 at.% Cu sample determined from the X-ray diffraction peak broadening is significantly smaller than the metal area determined from the sulfur capacity. This may be due to a particle size distribution very different from the other samples. Electron microscopy indicates that a considerable part of the copper is very finely dispersed and may not be observed by X-ray diffraction.

In view of the present results, it is difficult to understand why Dalmon (*8*) obtained results for Ni–Cu/SiO_2 catalysts which correspond to homogeneous metal particles without surface copper enrichments. The average metal particle sizes (7 and 15 nm) of the Dalmon samples were somewhat smaller than those in the present work (15–20 nm). However, in the present study, hydrogen chemisorption measurements were also carried out for reduced catalysts (Ni–Cu/Al_2O_3) with particle sizes close to the same range (7–9 nm), and also in this case the chemisorption capacity showed a sharp drop as the copper content increased.

The cause of the lack of surface copper segregation in the reduced samples of Dalmon (*8*) should probably be attributed to the higher temperature of reduction used by him. In Ref. (*8*) it is reported that samples with a copper content of less than about 40% were reduced at 940 K and those with more copper at 1270 K. It is interesting to note that Fig. 7 in Ref. (*8*) shows that the hydrogen uptake at 45 Torr as function of the copper content corresponds to two straight line segments connected by a drop at about 40% Cu. We suggest that the high temperatures used for the reductions make possible the incorporation of silicon atoms from the support into the surface of the alloy particles. The surface tension is thereby decreased sufficiently to eliminate the driving force for the surface segregation. This suggestion is supported by the work of Praliaud and Martin (*28*). They explained the results of their magnetic and hydrogen chemisorption measurements on silica-supported nickel catalysts reduced at 920 and 1180 K by assuming the formation of a surface and a bulk Ni–Si alloy, respectively.

Bajpai *et al.* (*5*) obtained hydrogen chemisorption results very similar to the present ones for a range of Ni–Cu/Al_2O_3 catalysts with particle sizes in the range 5–12 nm. Assuming that the conclusion of Dalmon about the homogeneity of the metal alloy particles was valid for their samples,

Bajpai *et al.* (*5*) suggested that the drop in hydrogen chemisorption capacity was due to an ensemble effect. Obviously, they did not realize the close agreement between their chemisorption results and those obtained for massive Ni–Cu alloy samples and that the "linear" chemisorption results of Dalmon are qualitatively different (see Fig. 2).

2. Carbon Deposition

2.1. Morphology. The equilibrium experiments as well as the electron microscopy observations show that the carbon formed on Ni–Cu/SiO_2 catalysts, in the temperature range 673–973 K, is mostly of the usual whisker type. The mechanism of growth of this type of carbon is generally believed to involve diffusion of dissolved carbon in the nickel (*1, 4, 23*). Copper does not affect the structure of the carbon formed up to a threshold content in the alloys which, in the present study, corresponded to 80 at.%. At this concentration a different structure is formed in which many threads of nearly amorphous carbon are attached to a single metallic particle. The metal particles in this structure are not pear-shaped, as typically observed in the whisker carbon. In contrast, they show many facets, each one connected to a filament (Fig. 4b). This "octopus" carbon was also found on sulfur-passivated nickel catalysts, above a sulfur coverage corresponding to approx. 70% of the saturation coverage (*2, 29*). As for the sulfur case, this could indicate a change in carbon nucleation at higher copper contents as a result of a blocking of the dissolution of carbon into nickel.

2.2. Reaction rates. Grabke and coworkers (*30, 31*) studied the decomposition of methane on α- and γ-iron and obtained the following expression for the rate of carbon deposition:

$$r_c = k_+ P_{CH_4} P_{H_2}^{-1/2} - k_- P_{H_2}^{3/2} a_c \qquad (12)$$

in which k_+ and k_- are the aggregated constants for the forward and reverse reactions, respectively, and a_c is the chemical activity of carbon dissolved in iron, shown to be proportional to the surface concentration of carbon in the case of α-iron, while deviations from proportionality were observed for γ-iron.

Grabke *et al.* showed that expression (12) was in good agreement with kinetic measurements, not only for α- and γ-iron but also for iron–nickel alloys with 10 and 20 wt.% nickel (*32*). Turkdogan *et al.*[1] concluded, however, from their carbon gasification measurements that the rate of the backward reaction is independent of the carbon content at high concentrations.

Detailed studies of the kinetics of the deposition and gasification of carbon on nickel with CH_4–H_2 mixtures have not been reported. Williams *et al.* (*33*) used expression (12) in discussing the influence of water vapor on the steady-state carbon activity of nickel films in flowing CH_4–H_2–H_2O mixtures. Lázár *et al.* (*34*) found that the deposition of carbon on nickel foils does not obey expression (12) at low carbon activities. They also reported that Grabke *et al.* found the rate of hydrogasification to be proportional to $P_{H_2}^2$. Figueiredo and Trimm (*35*) found the same hydrogen pressure dependence for the time-independent rate of hydrogasification of nickel foils and Ni/Al_2O_3 catalysts. Moreover, they observed that in the case of nickel foils, the rate of hydrogasification was proportional to the amount of carbon initially present, while no correlation was observed in the case of the supported catalyst.

In the present work, the amount of carbon formed on the catalysts was far greater than that reported by Grabke *et al.* The independence of the carbon content observed by Turkdogan *et al.*[1] might, therefore, be expected to apply to the present results.

The above observations suggest that the kinetic data obtained in the present work may be described by a modified version of expression (12)

[1] The results of Turkdogan *et al.* are referred to in Ref. (*30*).

$$r_c = (k_+ P_{CH_4} - k_-^* P_{H_2}^2)/P_{H_2}^\alpha. \quad (13)$$

In contrast to Eq. (12), the rate in Eq. (13) is independent of a_c. Furthermore, by introducing the exponent α ($\alpha < 0.5$), it is taken into account that the inhibiting influence of hydrogen is expected to be smaller than that observed by Grabke *et al.* for iron and iron–nickel alloys.

Expression (13) was fitted to deposition and gasification rate data for the catalysts corresponding to 1 and 10 at.% Cu. The results are shown in Figs. 6a and b, respectively, and the values obtained for the parameters are shown in Table 4.

It is seen that expression (13) gives a good description of the data at the lower hydrogen pressures. At higher hydrogen pressures the rates are higher than predicted, which indicates that an upper limit of the gasification rate is reached.

The hydrogen exponent α is found to be 0.3 for both catalysts, i.e., somewhat lower than the value $\alpha = 0.5$ obtained by Grabke *et al.* for iron and iron–nickel alloys, but higher than that indicated by Figueiredo and Trimm (*35*).

Expression (13) was also fitted to data obtained for the rates of carbon deposition on a $Ni/MgAl_2O_4$ catalyst at 923 K (*1*) and on a $Ni–Cu/Al_2O_3$ catalyst with 10 at.% Cu at 798 and 873 K (*36*) in a $CH_4–H_2$ mixture. The hydrogen exponents obtained in these two cases were $\alpha = 0.08$ and $\alpha = 0.22$, respectively, indicating that the α value may depend on the support material.

These observations, as well as the values obtained for α in the present work, show that the results for nickel and nickel–copper alloy catalysts cannot be explained in the same simple way as the results for iron. However, qualitatively, the present results indicate that hydrogen is inhibiting the surface dehydrogenation steps less strongly, or that the methane chemisorption step on supported nickel and nickel–copper alloy catalysts is slower than for iron, so that the latter step can become rate controlling for carbon formation.

TABLE 4

Carbon Deposition in $CH_4–H_2$ Mixtures, Rate Constants and Exponent of Eq. (13)

Cu at.%[a]	T (K)	$k_+ \times 10^{4}$[b]	$k_-^* \times 10^{4}$[b]	α
1	798	3.3	0.35	0.3
1	873	9.5	0.16	0.3
10	798	1.8	0.37	0.3
10	948	9.0	0.13	0.3

[a] $\frac{Cu}{Cu + Ni} \cdot 100$.

[b] Rates in s^{-1}. Pressures in kPa.

3. *Ensemble and Ligand Effects*

In the Ni–Cu catalysts, the nickel surface sites are surrounded by copper atoms, which cannot activate methane. If the effect of copper is just to dilute the nickel sites, the following equation may apply for the rate:

$$r = r_0(1 - x_{Cu})^k \quad (14)$$

in which k is the number of nickel atoms in the active ensemble, x_{Cu} the atomic fraction of copper in the alloy surface, and r_0 the rate in the case of pure nickel. If copper deactivates the neighboring nickel atoms (electronic ligand effect), k will be higher than the ensemble size (*37*).

If the active ensemble consists of more than one nickel atom and/or ligand effects play a role, the rate should drop more than the hydrogen chemisorption capacity (nickel area) when the copper concentration is increased.

Figure 5 shows that this behavior is observed for the alloy catalysts with 25 at.% Cu or more, but not for catalysts with less than 10 at.% Cu. This can also be observed in Fig. 8 (points without line) as CH_4 decomposition rates follow the strongly chemisorbed hydrogen curve until 10 at.% Cu and then fall by about one order of magnitude. The rate constants obtained for alloy catalysts with 10 at.% Cu or less in Table 4 show that the rate of carbon formation

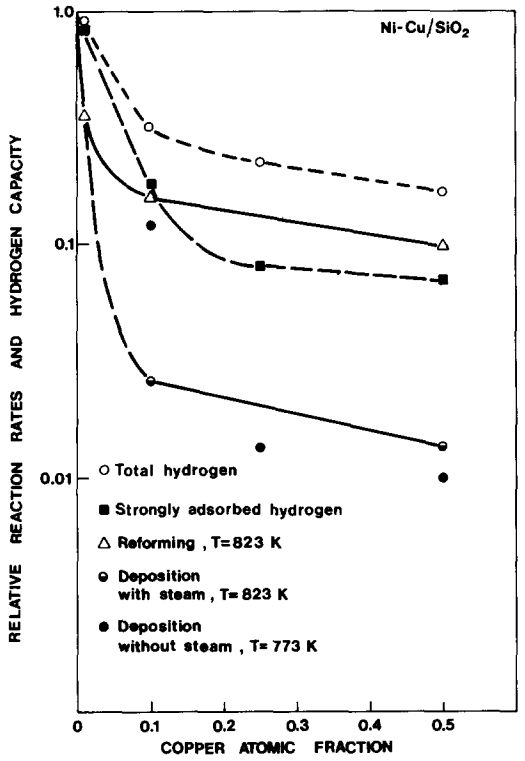

FIG. 8. Reforming and deposition rates relative to the rates for the 100% Ni/SiO_2 catalyst as functions of the copper content of the alloy catalysts. Also shown are the relative amounts of total and strongly chemisorbed hydrogen from Fig. 2.

decreases by less than a factor of 2, i.e., less than the drop in hydrogen chemisorption capacity, while the rate of gasification by hydrogen stays almost constant when the copper concentration is increased from 1 to 10 at.%. According to the Ponec classification (*12*), both processes thus belong to group I. This is consistent with the suggestion that chemisorption of methane or a surface reaction step is rate determining, as this implies the breaking of C–H bonds, which is typical of group I reactions. The strong decrease in the rate observed above 10 at.% Cu (Fig. 8) indicates a change to a group II reaction. This could be ascribed to a change in the rate-controlling step

$$CH_4 + *_n \xrightarrow{1} CH_x - *_n \xrightarrow{2} C - *_m \xrightarrow{3} C \text{ in Ni} \xrightarrow{4} \text{whiskers} \quad m > n \quad (15)$$

For low Cu contents the rates of steps, 2, 3, and 4 are high and step 1 becomes rate controlling. At high Cu contents the concentration of the larger ensembles, $*_m$, decreases more rapidly than $*_n$, and step 2 becomes rate determining. However, further studies are required to confirm this model.

4. Steam Reforming

The results obtained in the present work can be used to clarify the mechanism of simultaneous steam reforming and carbon deposition. The temperature dependence of the carbon deposition and gasification rates on Ni/SiO_2 is shown in Fig. 9. It includes the deposition of carbon in the absence (curve 1) and presence (curve 3) of steam and the gasification (curve 2) by steam. Curve 4 was obtained by subtraction of 1 and 2. Curves 1 and 3 were measured for

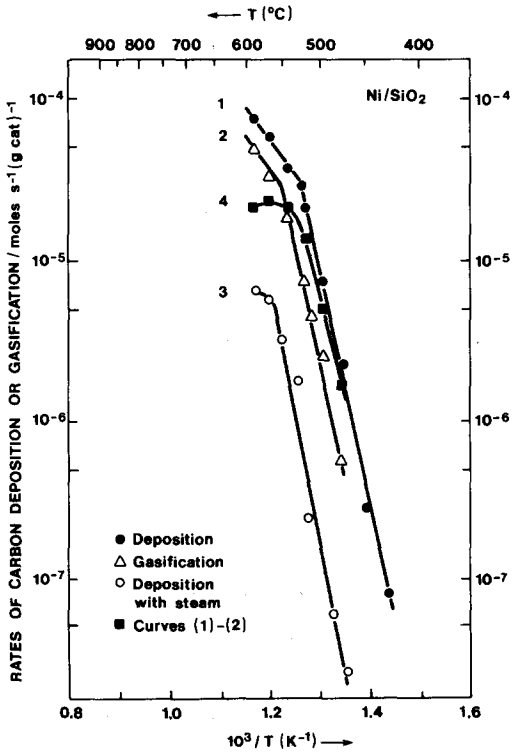

FIG. 9. Comparison of carbon deposition in the absence and presence of steam for 100% Ni/SiO_2 catalyst. Conditions: Curve 1: P_{CH_4} = 13.2 kPa, P_{H_2} = 7.1 kPa. Curve 2: P_{H_2} = 7.1 kPa, P_{H_2O} = 3.4 kPa. Curve 3: P_{CH_4} = 13.2 kPa, P_{H_2} = 7.1 kPa, P_{H_2O} = 3.4 kPa. N_2 as balance in all experiments. Total flow ca. 0.7 mol h^{-1}.

the same partial pressures of methane and hydrogen, and curves 2 and 3 for the same partial pressures of hydrogen and steam. Results similar to those in Fig. 9 were obtained for the 1 at.% Cu catalyst.

It can be concluded that the carbon monoxide and carbon dioxide formed during the reforming reaction do not originate from steam gasification of already-formed carbon deposits, since this would imply that curves 3 and 4 should almost coincide. It is true that hydrogen gasification also affects curve 1, but this cannot alter the previous conclusion, as this effect is minor in the presence of steam.

In the light of these ideas, it is interesting to discuss the occurrence of a common intermediate for steam reforming and carbon deposition. It has been suggested that this intermediate could be adsorbed carbon atoms (*2, 38*). However, on a catalyst with a lower concentration of nickel atoms, complete dissociation of methane may not be necessary for steam reforming (*2*).

In terms of sequence (15) it means that $CH_x - *_n$ may become the most abundant surface intermediate at higher copper contents and hence the intermediate for the reforming reaction, whereas the carbon deposition still requires $C - *_m$ as intermediate.

As can be observed in Fig. 8, the reforming rates follow closely the curve of strongly chemisorbed hydrogen (Type I reaction (*12*)), whereas the deposition rates are one order of magnitude lower (Type II reaction).

CONCLUSIONS

The main conclusions of the present work can be summarized as follows:

1. Silica-supported Ni–Cu alloy catalysts with one metallic phase can readily be obtained by "dry" impregnation if the catalyst contains more nickel than copper.

2. Copper surface segregation takes place in the same way on supported Ni–Cu alloy particles reduced at moderate temperature (~770 K) as on massive Ni–Cu alloys.

3. The carbon formation/gasification equilibrium in CH_4–H_2 mixtures is the same for Ni–Cu catalysts as for pure Ni catalysts except at very high copper contents (80 at.% Cu).

4. In the absence of steam the carbon deposition rate depends only weakly on the copper concentration when the copper content is low (10 at.% or less) and the observed dependences on hydrogen and methane pressure indicate that the chemisorption of methane and/or one of the first surface dehydrogenation steps is rate controlling. The copper concentration dependence is much higher when the copper content is above 10 at.%, indicating a change from a Type I to a Type II reaction, which can possibly be explained by an ensemble effect. At very high copper concentrations (80 at.% Cu) a new form of carbon filaments ("octopus" carbon) is seen in the electron microscope.

5. The rate of carbon formation in the presence of steam is significantly lower than expected from a simple superposition of the rate of carbon deposition without steam and the rate of gasification by steam. Different rate-determining steps appear to be involved in the reforming and carbon deposition reactions. The former can be considered as a Type I reaction. Deposition in the presence of steam appears to be a Type II reaction for all copper concentrations.

ACKNOWLEDGMENTS

The authors wish to thank Ulla E. Petersen, Ane M. Blom, and Steffen V. Christensen for technical assistance, Jørgen Villadsen for the X-ray work, Ole Sørensen for electron microscopy, and Bente Nielsen for fruitful discussions. C. A. Bernardo wishes to thank the Gulbenkian Foundation for a scholarship and the Universidade do Minho for granting leave of absence. Parts of the present work were carried out under NATO Research Grant 406/84.

REFERENCES

1. Rostrup-Nielsen, J. R., *in* "Catalysis, Science and Technology" (J. R. Anderson and M. Boudart, Eds.), Vol. 5, Chap. 1. Springer-Verlag, Berlin, 1984.
2. Rostrup-Nielsen, J. R., *J. Catal.* **85,** 31 (1984).

3. Frennet, A., and Lienard, G., *J. Res. Inst. Catal., Hokkaido Univ.* **16,** 115 (1968).
4. La Cava, A. I., Bernardo, C. A., and Trimm, D. L., *Carbon* **20,** 219 (1982).
5. Bajpai, P. K., Bakhshi, N. N., Dan-Chu, L., and Mathews, J. F., *Canad. J. Chem. Eng.* **60,** 613 (1982).
6. Barcicki, J., Nazimek, D., Grezegorczyk, W., Borowiecki, T., and Denis, A., *Pol. J. Chem.* **55,** 1839 (1981).
7. Khulbe, K. C., and Mann, R. S., *Catal. Rev.-Sci. Eng.* **24,** 311 (1982).
8. Dalmon, J. A., *J. Catal.* **60,** 325 (1979).
9. Vass, M. I., and Contescu, C. R., *Rev. Rom. Chim.* **25,** 55 (1980).
10. Maskos, Z., and van Hooff, J. H. C., *J. Catal.* **66,** 73 (1980).
11. Cale, T. S., and Richardson, J. T., *J. Catal.* **79,** 378 (1983).
12. Ponec, V., *Int. J. Quantum Chem.* **12,** Suppl. 2, 1 (1977).
13. Luyten, L. J. M., van Eck, M., van Grondelle, J., and van Hooff, J. H. C., *J. Phys. Chem.* **82,** 2000 (1978).
14. Dalmon, J. A., and Martin, G. A., *in* "Proceedings, 7th International Congress on Catalysis, Tokyo, 1980" (T. Seiyama and K. Tanabe, Eds.), p. 402. Elsevier, New York, 1981; *J. Catal.* **66,** 214 (1980); **75,** 233 (1982).
15. Dalmon, J. A., and Mirodatos, C., *J. Mol. Catal.* **25,** 161 (1984).
16. Sinfelt, J. H., Carter, J. L., and Yates, D. J. C., *J. Catal.* **24,** 283 (1972).
17. Iglesia, E., and Boudart, M., *J. Catal.* **81,** 204 (1983).
18. Gustafsson, L., *Talanta* **4,** 236 (1960).
19. Klug, H. P., and Alexander, L. E., "X-Ray Diffraction Procedures," Chap. 6. Wiley, New York, 1974.
20. Ponec, V., and Sachtler, W. M. H., *J. Catal.* **24,** 250 (1972).
21. Bénard, J., Oudar, J., Barbouth, N., Margot, E., and Berthier, Y., *Surf. Sci.* **88,** 135 (1979).
22. Geus, J. W., *in* "Materials Science Research" (G. C. Kuczynski, Ed.), Vol. 10, p. 29. Plenum, New York, 1975.
23. Baker, R., Barber, M., Harris, P., Feates, F., and Waite, J., *J. Catal.* **26,** 51 (1972).
24. Rostrup-Nielsen, J. R., *in* Proc. "Symp. on Science of Catalysis and Its Applications in Industry" p. XIII. FPDIL, Sindri, 1979.
25. Bernardo, C. A., and Trimm, D. L., *Carbon* **17,** 115 (1979).
26. Robertson, S. D., Kloet, S. C., and Sachtler, W. M. H., *J. Catal.* **39,** 234 (1975).
27. Soma-Noto, Y., and Sachtler, W. M. H., *J. Catal.* **34,** 162 (1974).
28. Praliaud, H., and Martin, G. A., *J. Catal.* **72,** 394 (1981).
29. Alstrup, I., Rostrup-Nielsen, J. R., and Røen, S., *Appl. Catal.* **1,** 303 (1981).
30. Grabke, H. J., *Metall. Trans.* **1,** 2972 (1970).
31. Grabke, H. J., and Martin, E., *Arch. Eisenhuettenwes.* **44,** 837 (1973).
32. Grabke, H. J., Müller, E. M., and Konczos, G., *Scr. Metall.* **14,** 159 (1980).
33. Williams, D. S., Möller, R., and Grabke, H. J., *High Temp. Sci.* **14,** 33 (1981).
34. Lázár, K., Kertész, K., Császár-Gilicze, É., and Konczos, G., *Z. Metallkd.* **71,** 124 (1980).
35. Figueiredo, J. L., and Trimm, D. L., *J. Catal.* **40,** 154 (1975).
36. Bernardo, C. A., Alstrup, I., and Rostrup-Nielsen, J. R., unpublished results.
37. Trolle Andersen, N., Topsøe, F., Alstrup, I., and Rostrup-Nielsen, J. R., in preparation.
38. Münster, D., and Grabke, H. J., *J. Catal.* **72,** 279 (1981).